Design of compact and low-power X-band Radar for mobility surveillance applications

Sergio Saponara, Bruno Neri

Abstract

This paper presents the design of a compact Radar for real-time detection of targets in smart mobility applications. The Radar integrates Fabry–Perot resonating antennas, X-band and configurable continuous wave transceiver, high-speed analog-digital-converter and low-power/low-cost FPGA for the baseband signal processing. The latter includes region-of-interest selection, 2D Fast Fourier Transform for range-Doppler map extraction, peak detection and alarm decision logic. The transmitted power can be configured from few mW to 1.8 W. This allows for a trade-off between the maximum detection range, from few hundreds of meters up to 1.54 km, and the Radar power consumption, from 2.56 W to 11.66 W. The measured speed is up to 40 m/s. The speed and distance resolutions are 0.3 m/s and 37.5 cm, respectively. The configurable Radar features increased robustness vs. laser-scanners, video cameras, or induction loops detection techniques, and stands for its better trade-off in terms of covered range, size, and low-power consumption vs. state-of-the-art surveillance Radars.

Keywords

Radar (Radio detection and ranging)
FPGA (Field Programmable Gate Array)
Smart mobility
X-band transceivers
Digital signal processing
Surveillance

1. Introduction

Robust sensing systems, tolerant to light and weather changing conditions, are required in smart mobility systems for surveillance applications or for driving assistance [1], [2], [3], [4], [5], [6], [7], [8], [9], [10], [11], [12]. Surveillance for

intelligent transport systems is needed in different scenarios such as railroad crossing [5], harbours [6], [7], [8], parking areas and roads [1], [2], [3], [4], [9], [10], [11], [12]. The sensing system can be integrated in the transport infrastructure or can be installed on board the vehicle: car, truck, bus or ships or even an UAV (unmanned aerial vehicle) for aerial surveillance [4] in smart cities. A Radar unit has the potentiality to allow for robust detection of targets and for the estimation of their motion conditions (speed, direction). The state-of-the-art is lacking designs of Radar units capable of long detection ranges, above 1 km, but with low cost, low size and low power consumption. A Radar is typically realized for defense applications or for the surveillance of big infrastructures or large areas (e.g. airports, large bay areas) [12], [13], [14]. However, the cost, size and power (e.g. 32 kW peak power in [14]) is too high for sensing applications in a potential large volume market, such as the smart mobility market. High transmitted peak power devices can create electromagnetic (EM) interference and pollution problems, and, due to health issues in dense populated urban scenarios, can overcome the EM emission limits fixed by law. On the other hand, single-chip and low-power Radar solutions have been proposed in literature: 60 GHz Radar sensor in [15] for proximity detection or UWB (Ultra Wide Band) Radar for vital sign parameter monitoring in [16], [17]. However, in these cases the covered range is few meters, not suited for surveillance mobility applications. To address these issues, this paper presents the design and test of a configurable Radar unit, embedding X-band radio frequency (RF) transceiver, analog-digital-converter (ADC) and FPGA-based digital processing blocks in a low-power and compact unit. The main technical contributions of this work vs. the state-of-the-art and vs. previous works of the authors [12], [18] are:

– The configurability of the maximum transmitted power, which allows for different trade-offs between the Radar power consumption and the maximum covered range (from 300 m to 1.54 km). This work features both a coarse-grained and a fine-grained configuration of the output power stage. The maximum transmitted power can be coarsly configured at 5 mW or 1.8 W. In the latter case a fine tuning from 1.8 W downto 700 mW can be applied to reduce the Radar power consumption. The maximum covered distance will be from 1.54 km at 1.8 W to 1.2 km at 700 mW.

–

Real-time implementation of signal processing tasks on the Artix-7 low-cost and low-power FPGA family, reducing power dissipation vs. state-of-the-art designs using GPU (Graphical Processing Units) and GPP (General Purpose Processors).

–

Radar parametric analysis, see Eqs. (1)–(16) in Sections 3 and 4, which highlights the inter-dependencies existing among Radar performance and analog and digital circuit parameters. This allows a co-design of the mixed-signal transceiver with the FPGA-based digital signal processing, and a trade-off between the Radar performance and its implementation complexity.

Hereafter, Section 2 compares the Radar sensing technology to other detection approaches. Section 2 also discusses the Radar specifications for smart mobility applications. Some examples are the monitoring of cars, pedestrians and bikers in a car parking, or the ingress/egress of ships in a small harbour. Sections 3 and 4 detail the design of the Radar transceiver and of the FPGA-based signal processing implementation. Moreover, Sections 3 and 4 discuss the trade-offs to be found between the Radar parameters and the performance requirements of the analog and digital circuits. Section 5 presents experimental results for some example applications and a comparison of the proposed Radar design with the state-of-the-art. Section 6 draws some conclusions.

2. Radar robust sensing

2.1. Radar sensing vs. other detection technologies

Radar technology, especially in the X-band (from 8 to 12 GHz), is preferable to other competing sensing technologies [6], [9], [10] for smart mobility, like video cameras, ultrasounds or laser-scanners, also known as Lidars (light detection and ranging). In a range from hundreds to few thousands of meters, Radar is much less sensitive to weather conditions than its competitors, allowing for a safe detection of obstacles during heavy rain, snow and hail, in presence of dense fog, strong sun glares and environmental noises and vibration. In Radar sensing, the detection and classification of a target is based on its Radar Cross Section (RCS). The RCS depends on the ratio between the power of the EM wave reflected by the target towards the Radar receiver, and the incident power on the target. The RCS is larger for targets made of conductive materials or very dense materials like stone and

wood. Radar imaging is preferable to other non-imaging technologies, such as induction loops and photoelectric or RF interruption beam sensors, because of its capability to monitor large areas with a great ease of installation, setup, use and maintenance. However, the widespread diffusion of Radar sensing requires the implementation at reduced size, weight, cost and power dissipation of the RF transceiver and the baseband signal processor. Table 1 summarizes the main properties of Radar sensing vs. other competing technologies for surveillance applications in transport systems. To increase the redundancy, robustness and type of services offered by intelligent transport monitoring system, the recent trend [9], [10] is realizing a fusion of the information obtained from different sensors.

Table 1. Sensing technology for target detection.

Detection technology	Radar	Lidar	Video	Induction loops
Easiness to install/maintain	Y	Y	Y	Large loop size
Not limited to specific materials	Y	Y	Y	Only metallic objects
Robust to bad weather condition	Y	Issues with fog/rain		Y
Robust to light/dark condition	Y	Y	N	Y

2.2. Radar specifications

When designing the Radar sensing system the following aspects have been considered. Concerning sensor size and weight, they should be limited to few tens of cm per side and to less than 10 Kg, especially for the installation on-board the vehicle (a car or a truck or an UAV). The typical targets to be detected in smart mobility scenarios are obstacles like vehicles (cars, bikes, ships, bus, trucks), people or animals suddenly crossing the road or the rail. For such targets the RCS is from few m^2, or even lower, to hundreds of m^2. The relevant materials are metal, wood, stone, heavy plastic and organic materials, easily detected by a Radar. People, vehicles, and other obstacles can either be still or moving with a speed up to 40 m/s, i.e. almost 150 km/h. This value, considered in this paper, covers applications in car parking, railroad crossing, movement of ships, road traffic in urban scenario and even in highway. Indeed, in most countries the speed limit is 36 m/s (130 km/h). Specific applications involving vehicles at very high speed, up to 80 m/s, such as high-speed trains or premium cars in a highway without speed limits (e.g. in German highways), are out of the scope of this work. These high-speed applications require narrow antenna beams and dedicated sensing solutions.

The detection range considered in this work is from few meters (urban scenario) to several hundreds of meters, e.g. 300 m in extra-urban roads. The detection range is above 1 km in maritime applications (e.g. traffic control of an harbour or monitoring of a bay area) or when monitoring large parking areas. The monitoring system has to work with different light conditions (night and day), with rain or fog or snow. For the target applications of this work the operating temperature is from – 40 °C to 85 °C.

Table 2 reports the main Radar sensor specifications. The X-band is a good working frequency choice, being a trade-off among sensor/antenna dimensions (the wavelength is few cm), working bandwidth, resolution, maximum covered range, effect of the weather conditions. At higher frequencies, such as the 60 GHz adopted in [15], [16], the peak absorption of oxygen drastically reduces the sensing range to few meters. At 24 GHz or at 77/79 GHz, adopted in [11], [19], [20], the design and development costs are increased due to the use of high-end devices in heterojunction technologies. Moreover, 24 GHz and 77/79 GHz automotive Radars are designed to be installed on-board the car with a coverage range of 10–20 m in short-range Radars, and a coverage range up to 200–250 m in long range Radars. Therefore, they are not suited for surveillance of large parking areas or harbours where a coverage range one order of magnitude higher, up to 1 or 2 km, is required. On the other hand, at frequencies below 10 GHz the wavelength increases and the size of the antenna and of the RF subsystem can become too high vs. the application requirements. A remarkable effect of the X-band choice is that, for the ranges of interest, rainfall, snowfall and fog cause negligible drawbacks on the detection function of the Radar because the wavelength is bigger than the water droplets and ice crystals involved in such weather phenomena.

Table 2. X-band Radar sensor specifications.

Type	B	Speed Res.	Speed Max	Distance Res.	Range Max	Output Power
LFMCW	0.4 GHz	0.33 m/s	40 m/s	37.5 cm	300 m	5 mW
					1.54 km	1.8 W

A Linear Frequency Modulated Continuous Wave (LFMCW) Radar is the most suited choice to keep low the power consumption and the EM interference. Differently from classic pulse Radars, emitting high peak power pulses (hundreds of Watts or even kWatts, e.g. 32 kW in [14]), the LFMCW Radar emits continuously much lower power levels without a relevant degradation of the Signal to Noise

Ratio (SNR). A configurable output power transceiver scheme is considered in this paper for the Radar, transmitting 5 mW for covered distances up to 300 m, and 1.8 W for distances up to 1.54 km. In this case a fine tuning from 1.8 W downto 700 mW can be applied to reduce the Radar power consumption. The maximum covered distance will be from 1.54 km to 1.2 km. These power levels, within 2 W, can be obtained with solid state power amplifiers, thus avoiding cumbersome and costly klystron, magnetron or other high-power high-frequency transmission systems typical of pulsed Radars [14]. The LFMCW technique entails a more complex digital processing chain, based on 2D FFT range–Doppler map extraction. However, it can be implemented in real-time in a low cost FPGA device family, as proved in Section 4.

The distance and speed resolutions of our design, 37.5 cm and 0.33 m/s respectively, were chosen taking care of typical vehicles and obstacles dimensions and motion characteristics, and of hardware performance requirements. A distance resolution of 37.5 cm is obtained by means of a 0.4 GHz bandwidth (B) sweep around an X-band central frequency.

3. Radar transceiver front-end

3.1. Radar transceiver architecture

Fig. 1 shows the architecture of the X-Band Radar, made of a mixed-signal front-end and an FPGA. The mixed-signal front-end includes transmitter (TX) and receiver (RX) antennas plus a FMCW transceiver with a high-speed ADC. The transceiver is implemented assembling COTS (Commercial Off The Shelf) integrated circuits on a microwave printed circuit board. The FPGA implements the digital signal processing chain. It also manages control tasks and the communications with external devices. The TX and RX channels of the transceiver exploit a LFMCW approach, giving information both on the distance d and on the radial velocity V_R of the target, by using low values of the output power. Received EM echoes are processed (see details in Section 4) by extracting range-Doppler maps. In a LFMCW system, see Fig. 2, the frequency is periodically swapped, with a linear law and within a time frame T_R, from f_{MIN} to a value $f_{MAX} = f_{MIN} + A \cdot T_R$.

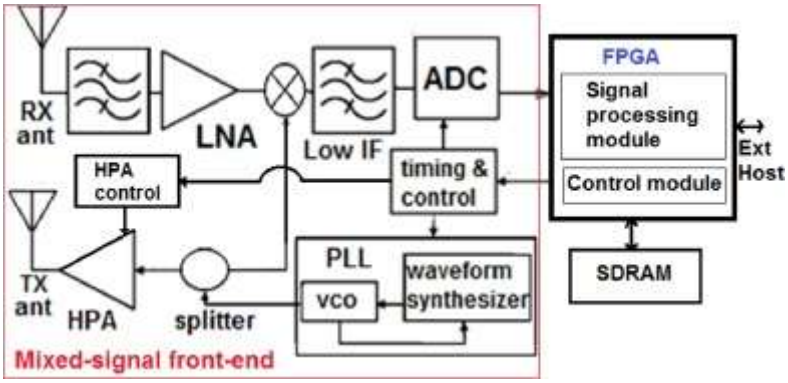

Fig. 1. Architecture of the X-band LFMCW Radar.

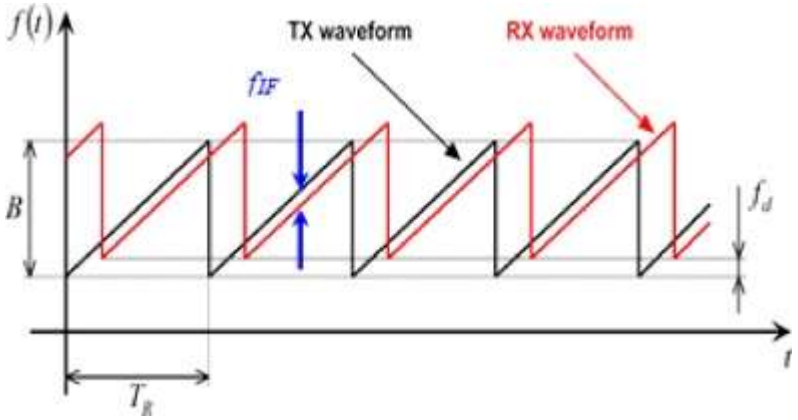

Fig. 2. LFMCW sawtooth waveforms; the f_{IF} contribution is due to target distance and relative speed (Doppler shift f_d).

The principle of operation of this Radar can be summarized as follows. The instantaneous frequency transmitted by the TX antenna in Fig. 1 is reported in Eq. (1). Whether a target at a distance d reflects the transmitted wave, the back scattered wave arrives at the receiving antenna with a delay $\tau = 2d/c$, being c the electromagnetic wave speed in the medium. The received frequency $f_R(t)$ at instant t is reported in Eq. (2). At the output of the mixer in Fig. 1, at time t, the frequency f_{IF} is equal to the difference between f_T and f_R, see Eq. (3).(1)fT(t)=fMIN+A·t,(2)fR(t)=fMIN+A·(t−τ)(3)fIF=fT(t)−fR(t)=A·τ=A·2d/c

By measuring f_{IF} the value of d can be evaluated, since A is a known parameter from Radar design. The difference between the maximum (f_{MAX}) and minimum (f_{MIN}) instantaneous value of the frequency, labeled B in Fig. 2, is sized depending on the required distance resolution d_R:(4)B=fMAX−fMIN=A·TR=c/2dR

Therefore, by targeting a distance resolution d_R better than 50 cm for smart mobility applications, B should be at least 300 MHz. By choosing a value for B of 400 MHz the achieved resolution is 37.5 cm in this work. The instantaneous frequency $f_T(t)$ is

generated in our scheme of Fig. 1 by a VCO (Voltage Controlled Oscillator), capable of operating with frequencies from 9.8 GHz up to 11.4 GHz, inserted in a PLL-based (Phase Locked Loop) waveform synthesizer [21]. To this aim, the RFVC1843 VCO by RFMD is integrated on the same microwave board with a Fractional N delta-sigma PLL capable of generating frequency ramps with sweeps of 400 MHz around a central frequency of 10.65 GHz in 100 µs. Therefore, the parameter A in Eq. (4) can be up to $4 \cdot 10^{12}\ s^{-2}$. The FFT computation time for each frequency ramp of the signal processor in Section 4 constraints the sweep time T_R at a value of 175 µs. Because of the co-design between the analog and digital parts, the parameter A in the waveform synthesizer is kept at $2.28\ 10^{12}\ s^{-2}$. Summarizing, we designed a continuous waveform generator based on a PLL with a VCO, sized for a chirp rate A of $2.28\ 10^{12}\ s^{-2}$, and operating around 10.65 GHz with $B = 0.4$ GHz frequency swap.

A fixed antenna is used to reduce system cost and size. Therefore, there are no moving parts in the proposed Radar unit. To realize compact and efficient antennas, both at TX and RX side, an X-band Fabry–Perot resonator technology, as in [22], is adopted. Fig. 3 shows the layout of the antenna (front and side views), whose size is about $7.2 \times 7.2\ cm^2$.

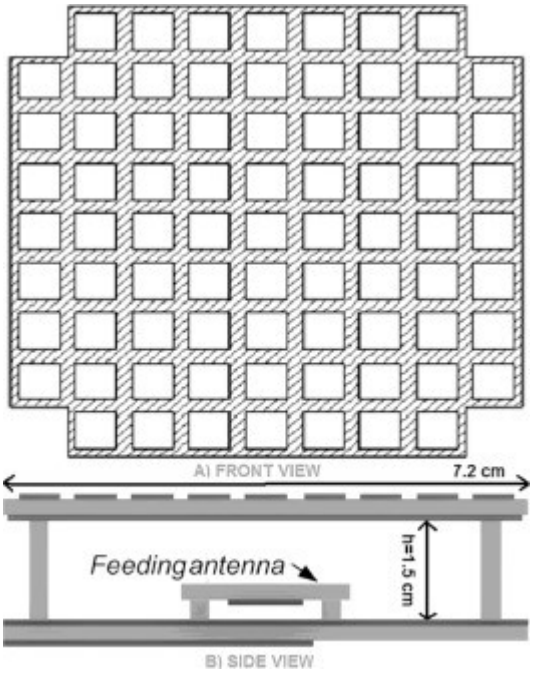

Fig. 3. Fabry–Perot resonating antenna. A) front, B) side views.

Square patches and apertures are etched on a Rogers RT/duroid 5880 substrate with a thickness of 0.787 mm and a dielectric constant of 2.2. By combining both TX and RX antennas, including a separating space of about 2.8 cm (which as discussed

in [22] allows reducing antennas coupling effects), a size of 7.2×17 cm^2 ≅ 120 cm^2 is obtained. Both the transmitting and receiving antennas have a gain (G) of at least 13 dBi, with a peak of 13.4 dBi. The return loss (S11 parameter of the antenna) is below −10 dB in the bandwidth of interest. The half power beamwidth is ± 30° in azimuth.

A maximum output power of 1.8 W (32.55 dBm) is obtained with the stage marked HPA (High Power Amplifier) in Fig. 1, realized using the HMC487 device plus a 50 Ω matching network with the transmitted antenna. In this work for the transmitted power we refer to the OP1dB (1 dB Output Power compression point). The OP1dB is the power level delivered by the amplifier when operating in a linear region, with a compression vs. an ideal amplifier below 1 dB.

The HMC487 power amplifier has an input noise figure of 9 dB and a gain higher than 20 dB in the bandwidth of interest. It gives the main contribution to the system power consumption, 9.1 W (1.3 A current from a 7 V voltage supply) having an efficiency of 21.5%. The OP1dB of the HMC487 power amplifier can be fine-tuned in the range from 0.7 W (28.45 dBm) to 1.8 W (32.55 dB) by regulating its supply current from the 7 V source, in the range from 850 mA to 1.3 A. Therefore, the contribution of the HPA block to the system power consumption will range from 5.95 W to 9.1 W.

A low-power Radar configuration is also designed, targeting a lower range without the HPA stage. In such case, the HPA in Fig. 1 is by-passed and the TX antenna is driven directly by the output of the VCO, which can provide up to 5 mW (7 dBm).

Concerning the receiver path in Fig. 1, its noise figure is less than 5 dB, whereas the LNA (Low Noise Amplifier) gain is 31 dB Further 43 dB of gain are obtained in the stage operating at intermediate frequency (IF) in Fig. 1. The 1 dB Input Power compression point (IP1dB) is −30 dBm. Fig. 4 shows the S21 parameter in dB of the first receiver stage, LNA plus the input filter. The return loss S11 is lower than −10 dB for a frequency range from 10.3 GHz to 11 GHz with a minimum of - 29 dB at 10.45 GHz. The LNA peak gain is 32.3 dB with a −3 dB bandwidth from 10.24 GHz to 11.05 GHz. In the frequency range of interest, 500 MHz around 10.65 GHz, the LNA gain is 31 dB and the return loss is below −10 dB

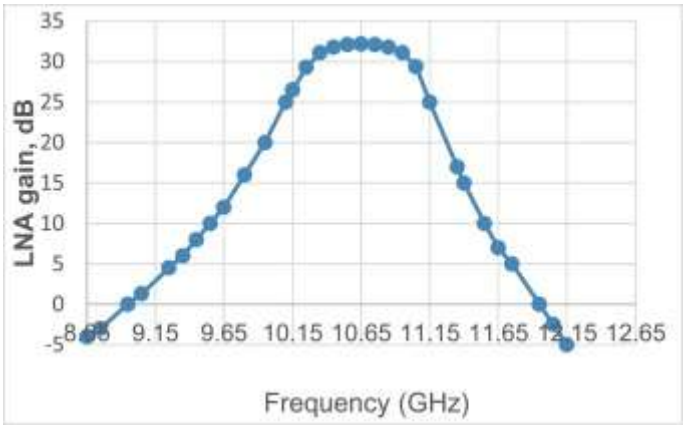

Fig. 4. Gain (S21) of the LNA and input filter.

In the configuration with the HPA stage, when transmitting 1.8 W towards targets at distance of few meters, the received signal is above the IP1dB point of the LNA. To avoid the relevant distortions, the peak of the received signal is detected in the analog transceiver and, if it is above a proper threshold, the HPA stage is bypassed.

Once fixed the parameter A to $2.28 \cdot 10^{12}$ s^{-2}, and the maximum and minimum distance of the target ($d_{max} = 1500$ m, $d_{min} = 1$ m), the IF bandwidth is defined from Eq. (3). Signals at f_{IF} are from 15.25 kHz up to 22.87 MHz. Knowing the spectrum of signals at IF is useful for the design of the ADC, which samples the data directly at IF.

An anti-aliasing filter is used before sampling the beat signal at a Nyquist-rate of 46 MHz (i.e. 46 MSa/s) with a commercial ADC device. The filter is a 6th order low-pass Chebyshev one. The selected ADC circuit is the AD9259, with up to 4 channels thus supporting Radar architecture extension to multiple channels. The AD9259 ADC has a pipeline architecture with the following characteristics: 14 bits/sample, sample rate up to 50 MHz per channel, 84 dBc Spurious Free Dynamic Range (SFDR), 72.7 dB Signal to Noise and Distortion Ratio (SINAD), 0.5 LSB (Last Significant Bit) differential non-linearity and 1.5 LSB integral non-linearity. The power consumption of one ADC channel is 2 mW in power down mode and 98 mW at maximum speed of 50 MSa/s. The power consumption for the whole mixed-signal front-end of the Radar, in the configuration with one transmitter, one receiver and including the contribution of the ADC operating at IF, is 2.4 W without the final HPA stage. In this configuration the VCO provides up to 5 mW at the TX antenna. Considering a configuration that includes also the HPA stage, the power consumption of the mixed-signal front-end is from 8.35 W (700 mW provided at the TX antenna) to 11.5 W (1.8 W provided at the TX antenna).

3.2. Doppler signal processing and SNR performance analysis

To process in the frequency domain the signal up to 46 MSa/s within a time window of $T_R = 175$ µs, an FFT of at least 8050 point is needed. An FFT with a power-of-two value of 8192 points is used for frequency analysis of the range signal in Section 4. Due to the Doppler effect, in case of moving targets, called *Vr* the relative speed between the Radar sensing node and the target, the frequency f_{IF} from Eq. (3) is shifted by the absolute value (*fd* in Fig. 2) calculated from Eq. (5).(5)fd=2·Vr/λ

This means that the information on the speed and on the distance of the target are both contained in the beat signal, at the output of the mixer in Fig. 1, according to Eq. (6).(6)fIF=−2·Vr/λ+A·2d/c

For a triangular LMFCW waveform, Eq. (6) is modified in Eq. (7) where two beat signals appear during up-chirp (positive ramp) sweep and down-chirp (negative ramp) sweep.(7)fIFupchirp=−2·Vr/λ+A·2d/c,fIFdownchirp=−2·Vr/λ−A·2d/c

In this work, λ is about 2.8 cm and the maximum considered relative speed of the target is 40 m/s. From Eq. (6) the frequency shift on f_{IF} caused by the Doppler effect is within the range ± 3 kHz, between 0 and 2859 Hz in absolute value.

The frequency domain digital signal processing chain discussed in Section 4 allows separate analysis of range and Doppler data. For Nyquist sampling of the Doppler information at least a sampling frequency of 5.718 kHz has to be used. The specification on the speed resolution, 0.33 m/s in our case, set the frequency resolution at about 23 Hz from Eq. (5). To process in the frequency domain a Doppler signal at 5.718 kHz with a resolution of about 23 Hz a 256-point FFT is required. To be noted that in scenarios such as urban mobility, car parking, port ingress/egress, railroad crossing where the speed is lower than 15 m/s, then the frequency shift caused by the Doppler effect is ±1 kHz at maximum.

The SNR at the output of the RF transceiver, see Eq. (8), depends on the following quantities:

- the output power of the continuous wave transmitter, P_{CW} in Eq. (8), which corresponds to the parameter OP1dB discussed in Section 3.1;
- the target cross section σ , e.g. 1 m^2 for a pedestrian;
- the transmitting and receiving antenna gain (both equal to the same value, $G = 13$ dBi in this work);
- the total loss *L*, which is obtained adding the air loss (L_{am}), about 0.07 dB/km at 10 GHz, and the loss inside the system (L_{sys}), 5 dB in this work;

–

the maximum distance R_P of the target;

the equivalent available total noise power spectral density $N_0 = kTN_F$ at the input of the receiver, where the Noise Figure N_F is 5 dB in this work, k is the Boltzmann constant, and *T is 300 Kelvin* in typical operating conditions;

the bandwidth B_F of the filter at the output of the mixer receiver.(8)SNR=PRXkTBFNF=PCWλ2G2(4π)31LσRP41kTBFNF

In the digital domain, the equivalent of the filter bandwidth B_F is the frequency resolution Δf of the FFT so that B_F has to be substituted by Δf in Eq. (8) thus obtaining SNR_{dig} in Eq. (9).(9)SNRdig=PCWλ2G2(4π)31LσRP41kTΔfNF

The SNR_{dig} in Eq. (9) can be further improved by a factor M, where M is the number of identical repetitions of the received signal, by integrating the output for a time $T_{INT} = M \cdot T_R$, being $T_R = 175$ µs in this work. In the proposed Radar design $1/\Delta f$ is de-facto equal to T_R, then in Eq. (10) $M/\Delta f$ is substituted by T_{INT}. In this work, the Radar has been sized to ensure a SNR_{out} higher than 15 dB at the maximum detection distance.(10)SNRout=M·SNRdig≅PCWλ2G2(4π)31LσRP4TINTkTNF

Fig. 5 shows the achieved SNR_{out} values from Eq. (10) as a function of the P_{CW}, from 700 mW to 1.8 W, when using a configuration with the HPA stage. Different values of T_{INT} and M are considered in Fig. 5, which lead to different curves. As discussed in Section 4, the value of M determines the size of the FFT used in the digital domain to process the range-Doppler matrix. Power-of-two values are considered for M (from 64 to 512 in Fig. 5) to simplify the FFT, which can be de-composed in a cascade of Radix-2 or Radix-4 computation stages.

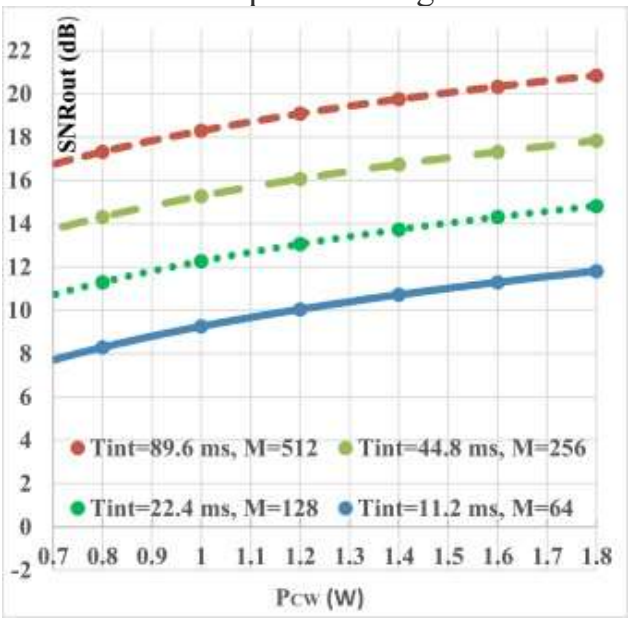

Fig. 5. SNR_{out} at the receiver side vs. transmitted power, after FFT signal processing and integration. 1.5 km range.

The curves in Fig. 5 are obtained considering a target with an RCS of 1 m^2 (e.g. a pedestrian) and a maximum coverage range $R_P = 1.5$ km. For targets having higher RCS, about 10 m^2 for a car, the SNR_{out} will be about 10 dB higher.

The results in Fig. 5 prove that, at a distance of 1.5 km, the Radar configuration with the HPA allows for a SNR at receiver side from 14 dB to 18 dB when the output power is increased from 700 mW to 1.8 W. These SNR values refer to an integration time of 44.8 ms ($M = 256$ repetitions). By doubling the integration time ($M = 512$) the SNR is further increased by about 3 dB, varying from 17 dB to 21 dB Fig. 6 shows the maximum target distance R_P that is detected by the Radar as function of the transmitted power, P_{CW}, when keeping the SNR_{out} as an input parameter, see Eq. (11). The curve in Fig. 6 corresponds to a SNR_{out} value of 18 dB In Fig. 6 the considered integration time T_{INT} is 44.8 ms ($M = 256$), whereas all the other parameters (kTN_F,σ, L, G, λ) are the same already used in Fig. 5. The results of Fig. 6 show that by tuning the transmitted output power of the HPA from 700 mW to 1.8 W the maximum distance at which a target is detected with a SNR_{out} of 18 dB varies from 1.2 km to 1.54 km.(11)Rp=PCWλ2G2(4π)31LσSNRoutTINTkTNF4

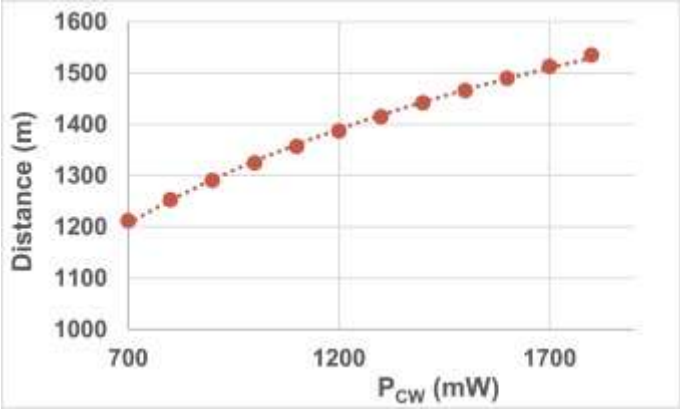

Fig. 6. Target distance vs. transmitted power for SNR_{out} of 18 dB.

Fig. 7 shows the achieved SNR_{out} values from Eq. (10) when the HPA stage in Fig. 1 is bypassed and the output power at the antenna, provided by the VCO, is up to 5 mW. In Fig. 7 the same parameters of Fig. 5 are considered, apart the target distance R_P that is 300 m. Fig. 7 shows that an SNR_{out} of 20 dB can be achieved at 300 m, with a transmitted power of 5 mW and an integration time of 44.8 ms ($M = 256$). Considering a minimum SNR_{out} value of 15 dB, from Fig. 7 it can be achieved with a transmitted output power of 1.5 mW.

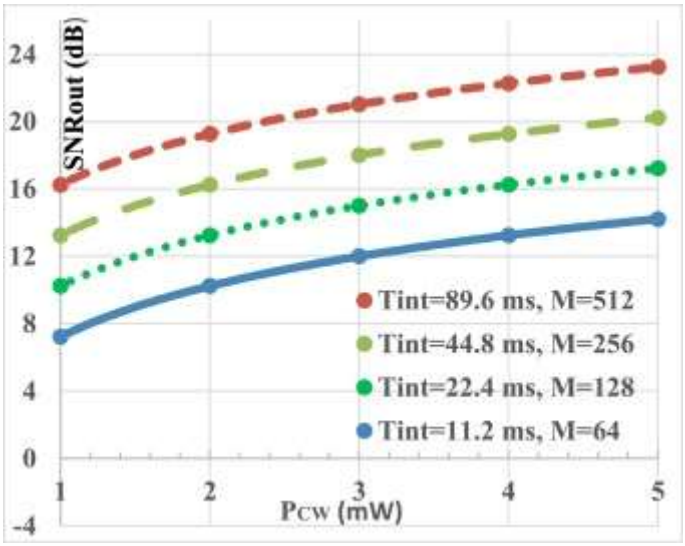

Fig. 7. SNR_{out} at the receiver side vs. transmitted power, after FFT signal processing and integration. 300 m range.

3.3. Radar module implementation

Before the hardware realization of the transceiver, several simulations are carried out both at the circuit and system level by using ADS (Agilent Technologies) CAD environment. For example, Fig. 8 shows the microwave board of the receiver. Receiver and transmitter sections are realized in separated boards to make easier the prototype test: they are contained in the same compact shielded case in the final system assembly. The case is connected to the TX and RX antennas and to the power supply. The low frequency output of the mixer, through Test Port in Fig. 8, after low pass filtering and amplification is made available for sampling and baseband signal processing on a FPGA-based board. The final Radar implementation is obtained by stacking at layer 1 the TX and RX antennas, at layers 2 and 3 one transmitter board and one receiver board, at layer 4 one board with the ADC plus the FPGA-based digital control and signal processing. The size of the Radar unit is about 120 cm^2, determined by the area of the two Fabry–Perot antennas. The weight of the Radar unit including the case is about 1 Kg.

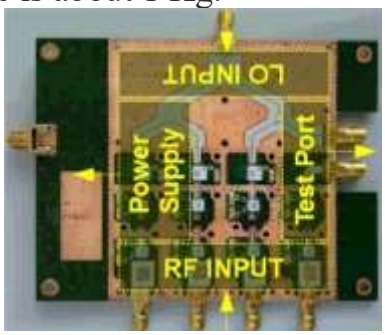

Fig. 8. Microwave receiver board of the LFMCW X-band Radar.

4. FPGA-based radar sensor signal processing

The whole digital signal processing chain of the Radar system (Signal Processing Module in Fig. 1) is implemented in a low-cost and low-power Artix-7 Xilinx FPGA. The same FPGA also manages the low-level interfaces of the system with the external world (Control Module in Fig. 1). The output of the Radar sensor analog unit in Section 3 is a baseband signal containing information about the monitored area. Such signal is digitally converted by means of the abovementioned 14-bit pipeline ADC, and processed by the FPGA-based section of the Radar to automatically detect possible targets inside the observation area giving information about range and radial speed of each target.

The core of the signal processing chain is a 2D FFT. First a 1D $N1$-point FFT is taken over each successive sweep of the sawtooth FMCW signal in Fig. 2. By chosing $N1 = 8192$ points and being 175 μs the sweep duration, each point of the sequence is at a time-distance of roughly 12.36 ns, which is de-facto the inverse of the maximum sampling bandwidth 46 MHz. The resulting transforms data are arranged as the rows of a matrix: a different row for each different sweep, i.e. M rows. A second set of 1D FFT is taken along the columns of the matrix whose number is $N1 = 8192$. Since in Fig. 5, Fig. 6 and 7 $M = 256$ repetitions (i.e. 44.8 ms integration time) allow for good SNR performance, then a $N2 = 256$-point FFT is applied along the columns. The Doppler-range matrix has a size 256×8192. Therefore, the analysis in Section 3.2 and in Fig. 5, Fig. 6 and 7 allows a co-design of the parameters of the digital part (FFT length size) with those of the analog part (transmitted power P_{CW}, antenna gain G, receiver noise figure N_F), taking care of functional metrics such as SNR and covered range.

Adjacent positions in the same column correspond to sample of the beat signal taken at T_R seconds each other. The columns of this matrix consist of elements of constant amplitude and increasing phase, which is proportional to the target Doppler shift f_D. The latter is easily derived by taking an FFT along the columns. The sweep period T_R defines the sampling period of the Doppler data. Its value should be related to f_D max and to Vr_{max} according to Eq. (12):(12)1/TR=2·fDmax=4·Vrmax/λ

Peaks along the rows in the frequency transformed domain will reveal the presence of a target and its range. Peaks along the columns in the frequency transformed domain will reveal the target relative speed. The frequency resolution resulting from the second FFT set, which evaluates the Doppler effect, is reported in Eq. (13) and is roughly 23.67 Hz in our Radar sizing. Therefore, from Eqs. (5) and (13) the

resulting speed resolution can be calculated from Eq. (14). Substituting the numerical values of the proposed Radar sizing the speed resolution amounts to 0.315 m/s, i.e. roughly 1.14 km/h.(13)$\Delta fD=1/(M\cdot TR)$(14)$\Delta V=\lambda\cdot\Delta fD/2=\lambda/(2\cdot M\cdot TR)=\lambda/(2\cdot TINT)$

From a computational cost point of view the main issue is represented by the fact that in a T_{INT} period, a 8192-point FFT has to be evaluated 256 times and a 256-point FFT has to be evaluated 8192 times. Since an N-point FFT needs about $N\cdot\log_2 N$ multiply and add operations, then in our case the two FFT processors will require roughly $44\cdot10^6$ multiply and add operations with fixed-point arithmetic for each T_{INT}. The number of multiply and add arithmetic operations per second is higher than 10^9. Considering that each complex data sample is digitized with 14 bits for the real and imaginary parts, then the transposition RAM needed for the 2D FFT processing (first 1D FFT along the rows, and then 1D FFT along the columns of the resulting matrix) when the Radar image is acquired for a period $T_{INT} = 44.8$ ms amounts to Mem_size = 256 × 8192 × 2 × 14 bits = 56 Mbits. To transfer the range-Doppler maps to an external host a data rate of at least Mem_size/T_{INT} is required. In our case study the data rate is higher than 1 Gb/s.

It can be demonstrated that the size of the range-Doppler map directly depends on the requirements in terms of:

– maximum range distance *dmax* and resolution *dr* for the number of columns (*Nc*) according to Eq. (15),

– maximum speed *Vrmax* and speed resolution *ΔVr* for the number of rows (*Nr*) according to Eq. (16).(15)$Nc=TR\cdot2\cdot fIFmax=TR\cdot4\cdot A\cdot dmax/c=4B\cdot dmax/c=2\cdot dmax/dr(16)Nr=M=\lambda/(2\cdot\Delta Vr\cdot TR)=4\cdot Vrmax\cdot\lambda/(2\Delta Vr\cdot\lambda)=2\cdot Vrmax/\Delta Vr$

To simplify FFT and memory design, if *Nc* and *Nr* are not power-of-two values, the nearest power-of-two values higher than the results of Eqs. (15) and (16) are selected. Reducing the system complexity just by reducing the range-Doppler map entails reducing the Radar system-level performances. To address the above hardware requirements for the digital unit of the Radar, while keeping low the implementation cost, an FPGA approach exploiting Artix-7 and Spartan6 device families is adopted. For the power consumption the target for the digital unit is bounding it to 1 W.

A computational cost higher than 10^9 multiply and add operations per seconds can not be addressed with low-cost/low-power microntrollers available on the market with 16 bit or 32 bit cores. Even specific Digital Signal Processors (DSPs) can fail in providing the required computational power. For example, in [23] two SHARC ADSP21062 are used for a range-Doppler matrix with a size halved vs. what proposed in this work. To achieve the same Radar performance in Table 1, up to 4 ADSP21062 processors have to be used in parallel for a single Radar channel. Supplied at 5 V the 4 ADSP21062 units have a power consumption of about 10 W.
FMCW Radar signal processing platforms using TMS320C6x DSP devices are proposed in literature [24], [25], e.g. TMS320C6747in [24] and TMS3206455 in [25]. However, in [24], [25] the DSP is always used in combination with FPGA co-processors, thus increasing the number of components, the area of the board, its cost, its power consumption. The TMS3206455 alone has a power consumption of 2.3 W at full speed.
The computational burden required for FMCW Radar signal processing can be sustained, as discussed in literature [12], by general purpose processors, e.g. core i7 [8], or GPUs [26]. However, such solutions entail a too high power consumption (tens to hundreds of Watts) not suited for the target compact Radar realization. On the other hand, the design of a custom integrated circuit (ASIC) with System-on-Chip (SoC) or Multi-Processor SoC (MPSoC) approach entails a too high time and development cost for the market of surveillance mobility, which is still not a large volume one. The ASIC approach represents a winning solution in case of large Radar channels (e.g. for direction of arrival estimation, phased arrays and digital beamformings and beam stearing in the digital domain) to be implemented at very low power budget, or when the Radar will become an ubiquitous adopted sensor in a large volume market.
At present, FPGAs for Radar signal processing and control offer the right trade-off between implementation cost and power consumption, signal processing capability and easy migration to ASIC approach in case of large volume market success or migration to a large number of Radar channels. Among the several available FPGA families, since this work aims at low-cost and compact Radar realization, Spartan 6 and Artix-7 device families are selected. Spartan6 FPGA devices are fabricated in 45 nm silicon technology, whereas Artix-7 FPGA devices are fabricated in 28 nm silicon technology. They have comparable cost, which is lower than other competing devices such as Kintex, Virtex or UltraScale families, to name just a few. Spartan 6

and Artix-7 devices are available with different qualification grades targeting different operating environments such as commercial (0°C–+ 85°C), industrial (−40°C–+ 85°C), automotive AEC-Q100 qualification and aerospace (−40°C–+ 125°C). The availability of qualified FPGA devices facilitates the migration of the proposed Radar system to several operating environments. The Spartan 6 FPGA family, with the XC6SLX100T device, offers about 63,400 LUTs (Look Up Tables) and almost 100,000 flip-flops for synthesis of combinatorial/sequential logic. In addition, it offers advanced features such as: on-chip integration of memory blocks (up to 4.8 Mbits, organized in 268 blocks of 18 kbits); dedicated DSP slices with 18 × 18 multiplier plus accumulator and adder (180 DSP slices in the XC6SLX100T FPGA); 4 SDRAM (Synchronous Dynamic Random Access Memory) controllers with data rates each up to 800 Mb/s; 8 Gigabit transceivers (GTPs) for I/O interfacing up to 3.2 Gb/s per channel; lots of differential I/Os up to 1 Gb/s; compatibility with PCI express or Gb/s Ethernet Interfaces; 12 Digital clock manager (DCM) and 6 PLL for multi-clock domain management and synchronization.

With respect to Spartan6, the new Artix-7 has similar resources in terms of LUTs, flip-flops, Gigabit transceivers, on-chip memory, DCM and PLL, but more DSP slices. The XC7A100T device has 240 DSP slices with a pre-adder, a 25 × 18 multiplier, an adder, and an accumulator. Thanks to the new 28 nm technology the Artix-7 family, although offered at comparable costs of the Spartan6, reduces power consumption by 60%. The processing algorithm is first prototyped in Matlab environment, and then translated in VHDL language. The resulting design is synthesized, placed and routed first on a Xilinx Virtex 6 FPGA and then optimized on low-cost Spartan6 and Artix-7 FPGA families.

The 2D FFT processor is implemented in hardware by synthesis of a VHDL architecture, which includes a cascaded mixed-Radix2/4 1D FFT core engine, with run-time configurable length. The 1D FFT engine is applied first along the rows, configured as a cascade of 6 Radix-4 stages and a final Radix-2 one, and then along the columns, configured as a cascade of 3 Radix-4 stages. A transposition RAM stores the 256 × 8192-cell matrix. Each basic Radix-4 operator implements in parallel, thanks to the butterfly operator in Fig. 9, up to 4 FFT operations involving multiplications and additions between a set of 4 input data and the relevant coefficients stored in a ROM (Read Only Memory). The architecture of the Radix-2

operator is a scaled version of that of Radix-4, since it processes in parallel 2 input data samples.

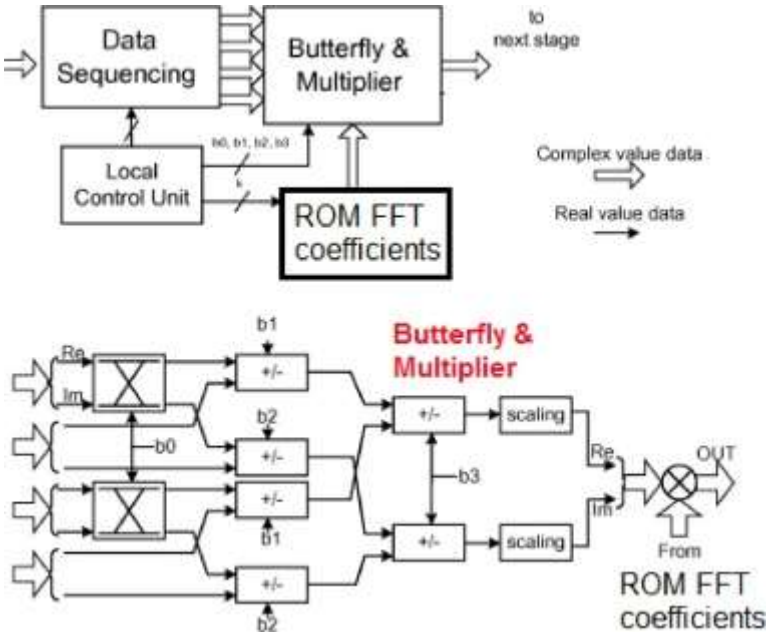

Fig. 9. Radix-4 operator at the core of the 1DFFT VHDL engine.

As reported in Fig. 10, a ping-pong strategy is used to pipeline the processing of the two 1D FFT processors. Otherwise, the speed of the 2D FFT processing will be limited by the fact that for Doppler estimation the 256-point FFT has to wait for the output results of the 8192-point FFT for range estimation. Thanks to ping-pong approach, while the 8192-FFT is processing a new sequence of input data, for range estimation, and stores the new results for each sweep by row in the memory M1, the 256-FFT is processing by column the data contained in memory M2. M2 was filled before by row with the output data of the 8192-FFT processor. At the end of each sweep time T_R, M1 and M2 memories are swapped. After memory swapping the 256-FFT starts processing by column the Doppler data from M1, while the 8192-FFT is processing a new sequence of input data, for range estimation, and stores the new results by row in the memory M2.

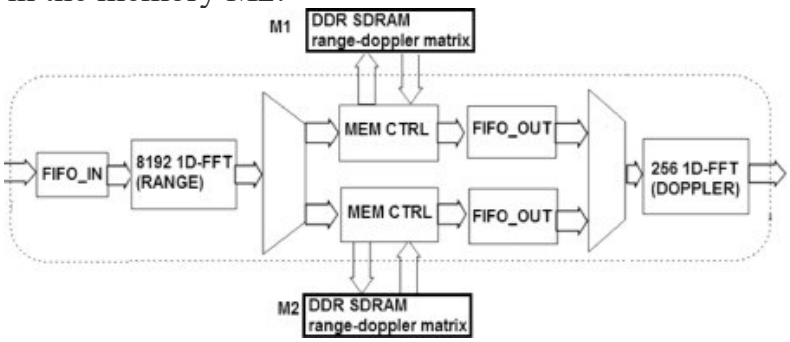

Fig. 10. Concurrent operation of the two 1D FFT processors thanks to ping-pong memory management.

Since 2 56 Mbits = 112 Mbits are outside the on-chip memory capability of low-cost FPGA families, such as the Spartan-6 or the Artix-7, then external SDRAM memory is required. The signal processing chain of the mobility surveillance system also includes other signal processing operators, beyond the 2D FFT. It can be divided in 6 main signal processing tasks, see Fig. 11:i) Data Gain Calibration, ii) ROI (Region-of-Interest) selection, iii) 2D FFT, iv) peak detection and first level detection, v) M/N second level detection, vi) alarm decision logic.

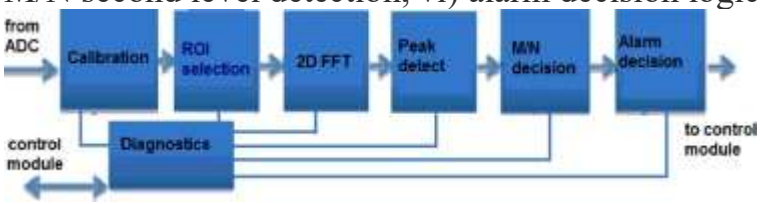

Fig. 11. Architecture of Radar imaging implemented on the FPGA.

The data gain calibration is a preliminary step, whose aim is calibrating the Radar signal to increase the robustness of the system to environmental variations that may occur during its functioning. In the ROI selection step sub-portions of the whole image can be defined to reduce the computational burden. Then the 2D FFT is applied: the output is an electromagnetic photography of the area of interest (e.g. railroad crossing, parking, small harbour) with peaks related to the presence of targets, their radial distance and speed.

On these areas a peak detection algorithm is applied to extract peaks having a power greater than user configurable threshold, each corresponding to a target characterized by a given range and radial speed. To find beat frequencies, a CA-CFAR (Cell-averaging Constant False Alarm Rate) detection algorithm [27] is applied to each frequency spectrum since CFAR can be efficiently implemented in FPGA. Fig. 12 shows the digital circuitry for the implementation of the CA-CFAR peak detection. Synthetizing this circuit on the FPGA resources requires less than 1 k flipflops and 200 LUTs.

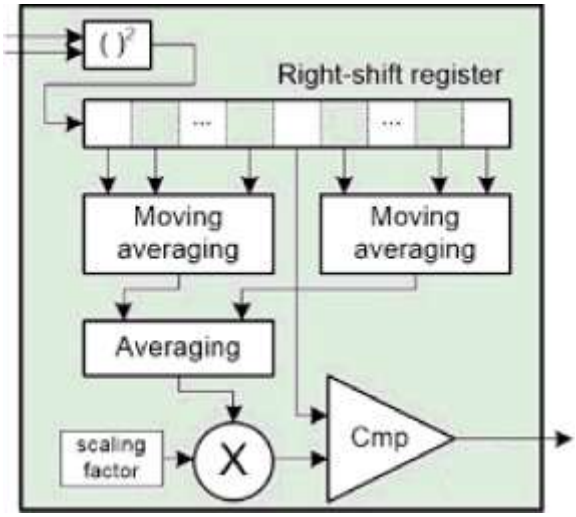

Fig. 12. CA-CFAR circuit for the peak detection in the Radar digital processing chain.

After peak analysis and first level of detection the task "M/N Second Level Detection" is applied. It implements a moving window detection logic to reduce the false alarm probability, given a target detection probability, granting at the same time a low response time when actually a target is present in the region of interest of the Radar. This task counts the number of the first level detections revealed by the previous task and signals the actual presence of an obstacle only if M first level detections occurred in the last N measurements.

Beside the digital signal processing part the FPGA includes a control module, which is a finite state machine, to provide proper configuration and timing commands to the other parts of the system (ADC, waveform synthesizer). The FPGA also manages low level HW interfaces of the system towards external SDRAMs, high-speed connection through the Gb/s transceivers, and low-speed differential I/Os to transfer to an external host the range-Doppler maps and alarms signals. To reduce bandwidth vs. the external host the range-Doppler map is transferred only for those sequences for which an alarm has been raised. To implement the calibration unit, a special loopback path is also implemented: the transmitted signal is routed through this path and sent back to be received, once digitalized, by the FPGA to perform the calibration operation as the antenna signal is received and to perform the diagnostics function. This unit also checks the coherency of the installation parameters, coming from the external interfaces and provides the thresholds to the peak detection and alarm generation units. The control module also implements a unit to write and read from an on-board FLASH memory. This allows for the storage of relevant processing intermediate outputs in a non-volatile memory, used to reload such data when needed (for example when restoring from blackouts). When designing the

FPGA, CENELEC-EN50128 guidelines for the development and test of safety critical software are taken into account. This includes the execution of simulations with statement and branch coverage besides static code analysis using automatic tools and synthesis flow verification.

All the control and signal processing part is integrated in a single Spartan XC6SLX150T device, which sustains in real-time the 256×8192 range-Doppler map processing with a clock frequency of 160 MHz. The 2D FFT latency, thanks to the ping-pong approach allowing concurrent operations of the two 1D FFT processors, which operate on separate data memories, is 155 µs. Considering also the implementation of the peak estimation and alarm detection we are able to process each FMCW sweep within the time frame $T_R = 175$ µs. The % of FPGA occupation is reported in Table 3. The bottleneck for the design of the FMCW Radar digital part on the FPGA is the use of the DSP slices with dedicated multiplier. The power consumption at 160 MHz with these resource occupations for the XC6SLX7150T device is roughly 630 mW. Given the results of Table 3 also other devices like the XC6SLX7100T can sustain the signal processing and control modules of the proposed Radar. In such case the power consumption for the digital part is 590 mW.

Table 3. Occupation of the Spartan6 and Artix-7 devices for FMCW Radar range-Doppler processing.

Device	FF	DSPslice	LUTs	Mem block
SLX100T	15.42%	83%	20.14%	25.1%
SLX150T	10.6%	83%	13.83%	25.1%
A35T	26.4%	58.8%	28.84%	80%

Repeating the same design on Artix-7 thanks to an higher number of DSP slices, and to a higher working frequency at 200 MHz, (due to the scaled 28 nm technology vs. the 45 nm technology of the Spartan6), 1 TX and 1 RX channel can be implemented in real-time on XC7A35T device. Implementation results (% of occupied FPGA resources) are reported in Table 3. The power consumption of the Radar processing implementation on the XC7A35T is 160 mW.

The total power consumption (analog and digital parts) for the X-band Radar with 1 transmitting channel, 1 receiving channel, real-time processing on a XC7A100T FPGA, and by-passing the HPA stage of Fig. 1, is 2.56 W. The Radar system performances are $d_{max} = 300$ m (with an SNR_{out} of 20 dB, see Fig. 7), $d_r = 37.5$ cm, $Vrmax = 40$ m/s, $\Delta Vr = 0.315$ m/s.

By adding the contribution of the HPA stage, and tuning its output power from 700 mW to 1.8 W, the total power consumption of the Radar is reported in Fig. 13 and is in the range from 8.44 W to 11.66 W. The Radar system performance in terms of maximum distance d_{max} and of SNR_{out} are those reported in Fig. 6. The other parameters $d_r = 37.5$ cm, $Vrmax = 40$ m/s, $\Delta Vr = 0.315$ m/s are the same. For a small series Radar production the total cost for the devices (active and passive, discrete and integrated), and for the realization of the boards and of the case, is in the order of some hundreds of euros.

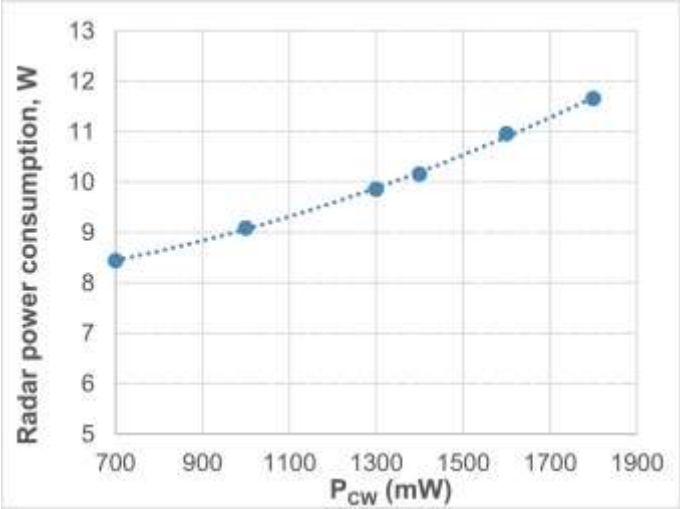

Fig. 13. Radar power consumption vs. HPA output power tuning.

5. Smart mobility applications and state-of-art comparison

5.1. Example applications to smart mobility

Using the Radar module presented in previous Sections, two different FMCW Radar configurations can be implemented, operating in the X-band for surveillance in mobility systems. The first configuration is for monitoring ships ingress/egress in small harbours or cars in large parking area, targeting a range up to 1500 m with a distance resolution of 37.5 cm. The measured vehicle speed is up to 40 m/s and the speed resolution is roughly 0.3 m/s. The signal processing is implemented in real-time on Artix-7 device. By enabling the use of the HPA, and configuring it for an output power transmission of 1.8 W, the total power budget is 11.66 W and the SNR at maximum distance is 18 dB The Radar can be contained in a case whose area occupation is about 120 cm^2. The second Radar configuration is obtained from the first one by-passing the HPA stage. It can be used for monitoring cars parking

or railroad crossing with a detected range of 300 m (with an SNR of 20 dB) while keeping unchanged all the other parameters. The power budget is 2.56 W.

The first Radar configuration has been tested on real scenarios for the surveillance of harbours, such has the ingress/egress of ships of different materials (wood and iron, fiberglass and iron, just wood) on the harbour of the naval academy in Livorno, Italy in a NATO contest in collaboration with the CNIT RASS laboratory [28] during a cloudy day. For example, Fig. 14 shows the range-speed map obtained during a test with 3 targets entering (target B), leaving (target A) or moving around (target C) the small harbour within a distance of 1500 m and a speed in the range ± 7 m/s. The colors from blue to red represent the detected power spectral density with a variation of 80 dBm from blue (minimum) to red (maximum). Fig. 15 shows in details the target B of Fig. 14 after ROI selection.

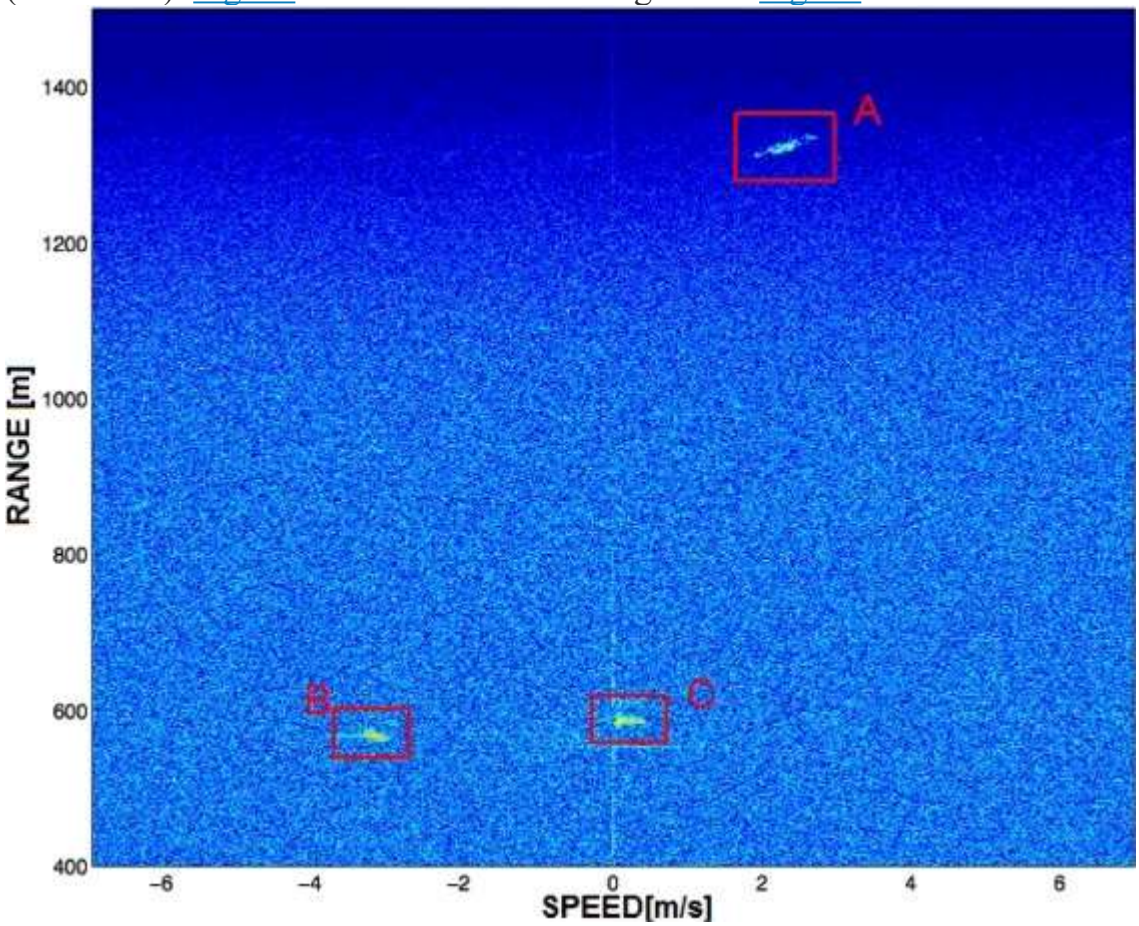

Fig. 14. Target detection of 3 ships in a small harbour, P_{CW} = 1.8 W.

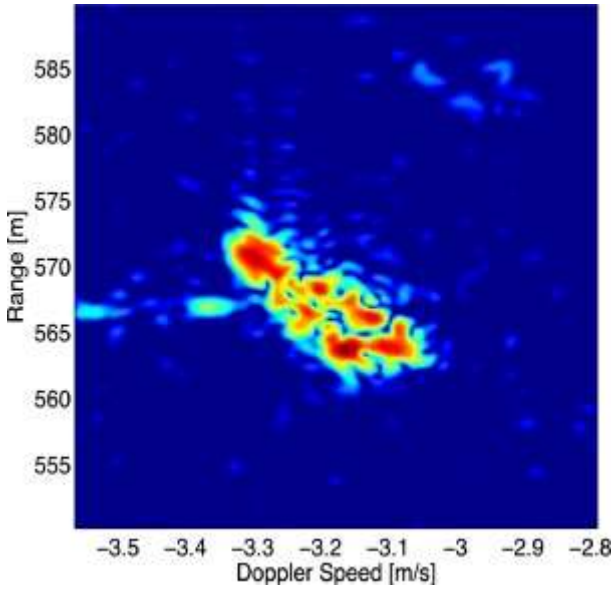

Fig. 15. ROI selection of target B.

By using the Radar configuration without the final HPA stage, a test campaign has been carried out in a car parking of the city of Pisa during a day with cloudy and windy weather. Fig. 16 shows example results. Three different targets have been detected: targets A and C are cars used in the test at distances at 125 m and 79 m respectively with a speed of −19 km/h for Target A, which is approaching, while C starts moving at few km/h. Instead, the Target B at 43 m distance and −5 km/h is a person cycling in the car parking.

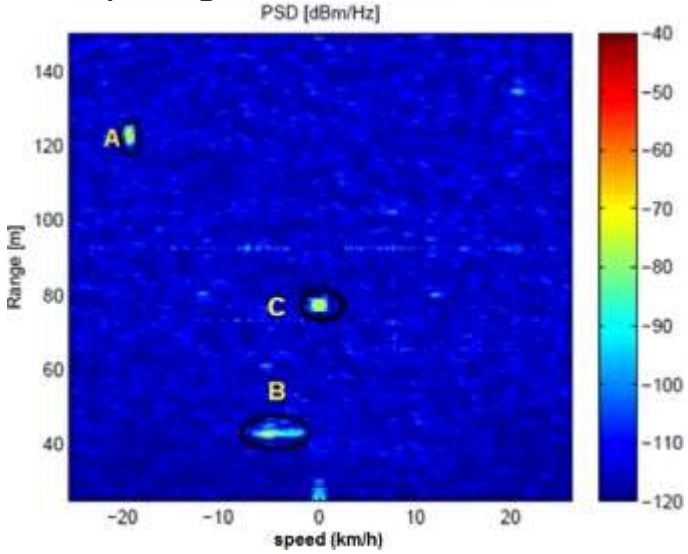

Fig. 16. Target detection in a car parking, P_{CW} = 5 mW.

5.2. Comparison to the state-of-the-art

Presented results show that the proposed Radar allows detecting moving and still targets in different mobility services like cars parking or ingress/egress of ships in a

small harbour. The proposed Radar unit allows for increased robustness vs. light conditions changes and weather changes when compared to other state of art works using Lidar, camera or ultrasounds imaging [6], [9], [10].

Table 4 compares the proposed solution to other Radar solutions recently proposed in literature. Several low power platforms have been presented in literature: e.g. the proposal of reusing for Radar the 60 GHz front-end and the powerful DSP processor already available in the next smart phone generation [15]. 60 GHz Radars pay the compact size and low-power consumption advantages in terms of a detection range of few meters, not suitable for mobility surveillance applications. Indeed, the peak of absorption of oxygen for electromagnetic waves at 60 GHz limits the use of such spectrum range to very short distances. Other works, based on a UWB approach, have been proposed in literature [17] for contactless measurements of vital parameters such as heart-rate or breathe-rate. Operating in the spectrum range from 3.1 to 10.6 GHz, these designs typically are optimized to cover a range of few meters and very low speeds but very high resolutions (hearth or chest displacements of few cm).

Table 4. Comparison to the state-of-the-art.

	Freq, GHz	Type	Power consumption	Range	Output power
This work	10.4–10.9	FMCW	2.56 W	300 m	5 mW
This work with HPA	10.4–10.9	FMCW	8.44 W	1.2 km	0.7 W
			9.56 W	1.4 km	1.2 W
			11.66 W	1.54 km	1.8 W
[11]	76–77	FMCW	4 W	250 m	5 mW
[17]	3.1–10.6	PulsedUWB	73 mW	<1 m	7 pJ/pulse
[15]	60	FMCW	N/A	< 3.5 m	N/A
[19]	22–26	PulsedUWB	N/A	N/A	2 mW
[13]	12–18	Pulsed	130 W	4 km	8 W
[14]	9.375	Pulsed	N/A	45 km	32 kW
[8]	9.5–9.8	FMCW	>100 W	3 km	5 W
[7]	10.5–10.8	FMCW	>100 W	1.2 km	2 W
[24]	2.48–2.56	FMCW	N/A	100 m	100 mW
[29]	9.2–9.5	FMCW	N/A	50 km	100 W
[30]	9.4	N/A	650 W	50 km	100 W

Automotive Radars, exploiting FMCW or pulsed UWB approaches, have been proposed in literature for Automatic Cruise Control working at 24 GHz or

77 GHz [11], [19], [20]. However, such works typically adopt ASIC approaches in heterojunction technologies resulting in high development time and costs, particularly for low or medium volume markets. Their output power is limited to few dBm. Hence, these works are suited for applications up to 100–200 m, but can not be used to control ingress/egress of ships in a harbour or large parking areas where the range to be covered can be several hundreds of meters. For these works, even adopting a dedicated power amplifier stage would be difficult to reach distances up to 1500 m since the attenuation of propagation is much higher than the attenuation in X-band. According to ITU-R P.676-4, the combined attenuation for air and water vapour is 0.3 – 0.5 dB/km in the 76–77 GHz band while for the X-band is one order of magnitude lower. With respect to the above works, the proposed Radar has performances, proved in real scenarios (detection range up to 1500 m or 300 m with/without the HPA stage, resolution of 37.5 cm, radial speed detection up to 40 m/s), suited for smart mobility surveillance applications in land or maritime environments.

With respect to X-band Radars such as [7], [8] adopting a general purpose processor for FMCW signal processing, e.g. Intel Corei7 CPU 860 at 2.8 GHz with 16GB DDR3 RAM in [8], in this work the FPGA-based computation reduces power consumption by one order of magnitude. Power is reduced from roughly 100 W in [7], [8] to less than 12 W when using the HPA stage. Moreover, while in [7], [8] transmitted output power is fixed, in this work we foresee the possibility of bypassing the HPA stage. In such case is the VCO chip that provides up to 5 mW to the TX antenna. The maximum detection range is 300 m, but the Radar power consumption is limited to only 2.56 W.

It is worth noting that, with respect to the X-Band Radar in Chapter 6 of [12], this work refers to a complete Radar solution (TX and RX antennas plus transceiver, ADC and FPGA real-time signal processing), whereas [12] describes only the transceiver. Particularly, [12] misses the design of the antenna, of the ADC and of the FPGA-based digital signal processing and control. With reference to the transceiver, the only block in common between this work and [12] is the receiving channel. The waveform synthesizer in [12] is sized for a bandwidth of 300 MHz, which allows for a resolution of 50 cm. Instead, in this work the FMCW bandwidth is increased to 400 MHz, which allows for a better resolution of 37.5 cm. Moreover, the power amplifier in [12] refers to a transmitted power up to 10 W, whereas this work implements a configurable solution allowing for different trade-offs between

Radar performance (maximum target distance and output SNR) and overall power consumption. From a theoretical point of view the work in [12] presents only a subset of the Equations considered in this work in Sections 3 and 4, and particularly considers only those related to the analog transceiver sizing.

Analyzing the literature of long-range surveillance Radars, most of them [13], [14], [29] are sized for much higher peak power. For example, the pulse compression Radar in [13] operating in Ku-band with a transmitted power of 8 W has a detection range from 20 m to 3.7 km. The range resolution is 5 m. The total power consumption is 130 W and the weight 35 kg. Therefore, a gain in the maximum range of factor 2.5 in [13] vs. our design (with the HPA), is paid in terms of detection resolution, weight and power consumption with performance reduction in [13] by more than one order of magnitude. The Radar in [14] has a 32 kW peak power, which allows for a 45 km covered range, but it is not suited for applications with limited budgets in terms of cost, power consumption, size and weight. The Radars in [29], [30] operate in X band and have a detection range of 50 km. However, they have a coarse resolution of 15 m in [29] and 50 m in [30], not suitable for mobility surveillance applications. In [29] the long detection range is obtained thanks to a transmitted power of 100 W and an antenna with a gain of 38 dBi, but with an antenna area of 7850 cm^2. In [30] the transmitted power is 100 W and the whole Radar has a weight of 68 kg, a power consumption of 650 W and a volume size of about 1 m^3.

Instead, this work allows for a more compact design, since the antenna we propose has a size 150 times lower (area of 51.84 cm^2) than [29], the transmitted power is 50 times lower than [29], [30], the total power consumption is two orders of magnitude lower than [30]. This way our solution avoids cumbersome cooling system and power supply unit. The proposed Radar follows a co-design and co-optimization approach when sizing the parameters for the analog transceiver, the mixed-signal ADC and the FPGA-based signal processing, whereas in literature the signal-processing platform [8], [23], [24], [25], [26] usually is designed independently from the analog transceiver.

6. Conclusions and future work

The paper has presented design and experimental test results for a compact, real-time and low-power Radar platform for smart mobility applications in terrestrial and nautical scenarios. According to a co-design approach, the Radar includes an X-

Band multi-channel FMCW transceiver with configurable output power, Fabry–Perot resonating antennas, FPGA-based real-time signal processing and communication unit. The configurability of the maximum transmitted power is a key feature of the proposed solution since it allows for different trade-offs between the system power consumption (from 2.56 W to 11.66 W) and the maximum covered range (from 300 m to 1.54 km). This work features both a coarse-grained and a fine-grained configuration of the output power stage. First, the transmitted power can be coarsely configured at 5 mW or 1.8 W. In the latter case, a fine tuning from 1.8 W down to 700 mW can be applied to reduce the Radar power consumption to less than 8.5 W. The maximum covered distance will be from 1.54 km to 1.2 km for a SNR_{out} of 18 dB To be noted that FMCW Radars operating with a SNR_{out} of 12 dB have been already proposed in literature for automotive applications [1]. Therefore, the considered 18 dB of SNR_{out} is a good compromise between circuit complexity and signal quality. Presented results show that the Radar unit allows detecting the presence and speed of moving and still targets in different mobility services like safe monitoring of car parking and ingress/egress of ships in a small harbour. The achieved performances are a covered range of 1.54 km with an output power of 1.8 W and, in a low-power Radar configuration, 300 m with an output power of 5 mW. The Radar can be embedded in a compact case, whose area size is about 120 cm^2 (more than one order of magnitude lower than X-band Radar solutions in literature [29]), and easily mounted on-board land, nautical or even aerial vehicles (e.g. UAV). Range resolution is 37.5 cm and the detectable speed is up to 40 m/s. The proposed Radar allows for increased robustness vs. light conditions changes and weather changes with respect to other detection technologies such as Lidar, camera or ultrasounds imaging. The proposed Radar stands for its better trade-off in terms of covered range, power consumption and size vs. state-of-the-art pulsed or FMCW Radars. The Radar can be connected as a node to a network of sensors, thus enabling data fusion in advanced monitoring systems. As a future work, to detect the exact position of targets, or even to reconstruct their shape in 3D, multiple receiving channels have to be used: at least 3 channels to solve azimuth and elevation DOA (direction of arrival). In this case the scheme proposed in this work must be scaled by adding at least 2 receiving channels at the A/D converter input.

Acknowledgments

Discussions with S. Lischi, R. Massini, D. Staglianò, F. Berizzi, M. Martorella (CNIT RASS), P. Ruggiero, M. Righetto (IDS spa) are gratefully acknowledged.

References

V. Issakov

Microwave circuits for 24 GHz automotive radar in silicon-based technologies
Springer (2010)
Google Scholar

M.A. Lalimi, S. Ghofrani, D. McLernon

A vehicle license plate detection method using region and edge based methods
Comp Electr Eng, 39 (3) (2013), pp. 834-845
ArticleDownload PDFView Record in ScopusGoogle Scholar

B.-F. Wu, H.-Y. Huang, C.-J. Chen, Y.-H. Chen, C.-W. Chang, Y.-L. Chen

A vision-based blind spot warning system for daytime and nighttime driver assistance
Comp Electr Eng, 39 (3) (2013), pp. 846-862
ArticleDownload PDFView Record in ScopusGoogle Scholar

H. Zhou, H. Kong, L. Wei, D. Creighton, S. Nahavandi

Efficient road detection and tracking for unmanned aerial vehicle
IEEE Trans Intell Transp Syst, 16 (1) (2015), pp. 297-309
View Record in ScopusGoogle Scholar

R. Ramchadran, J.T.J. Prakash

FPGA based SOC for railway level crossing management system
Int J Soft Comput Eng, 2 (3) (2012), pp. 134-137
View Record in ScopusGoogle Scholar

T.C. Glaser, N. Nino, K.A. Kramer, S.C. Stubberud

Submarine port egress and ingress navigation using video processing
Proceedings of the IEEE 9th international symposium on intelligent signal processing (2015), pp. 1-6
CrossRefGoogle Scholar

S. Lischi, R. Massini, D. Staglianò, L. Musetti, F. Berizzi, B.,MartorellaM. Neri

X-band compact low cost multi-channel radar prototype for short range high resolution 3D-InISAR
Proceeding of 11th IEEE European radar conf. (2014), pp. 157-160
CrossRefView Record in ScopusGoogle Scholar

S. D, E. Giusti, S. Lischia, M. Martorella

3D Inisar-based target reconstruction algorithm by using a multi-channel ground-based radar demonstrator
Proceeding of IEEE international radar conference (2014), pp. 1-6
View Record in ScopusGoogle Scholar

A. Roy, N. Gale, L. Hong

Automated traffic surveillance using fusion of Doppler radar and video information
Math Comput Model, 54 (1) (2011), pp. 531-543
ArticleDownload PDFView Record in ScopusGoogle Scholar

F. Laghezza, F. Scotti, M. Scaffardi, A. Bogoni, D. Onori, V. Vercesi, *et al.*
Integrated multi-frequency lidar/radar system for precise and robust Doppler measurements
Proceeding of the IEEE radar conference (2015), pp. 1109-1113
View Record in ScopusGoogle Scholar

J. Hasch, E. Topak, R. Schnabel, T. Zwick, R. Weigel, C. Waldschmidt

Millimeter-wave technology for automotive radar sensors in the 77 GHz frequency band
IEEE Trans Microwave Theory Tech, 60 (3) (2012), pp. 845-860
CrossRefView Record in ScopusGoogle Scholar

S. Saponara, E. Ragonese, M. Greco, B. Neri, G. Palmisano

Highly integrated low-power radars
Artech House (2014)
Google Scholar

Terma A/S. Scanter 1002 Ground Surveillance Radar, http://www.terma.com/media/262886/43193_terma_scanter_1002_letter.pdf; 2016 [accessed 03.06.2016].
Google Scholar

Terma A/S. SLAR9000: Side looking airborne radar, http://www.terma.com/security-surveillance/radar-systems/slar/; 2016 [accessed 03.06.2016].
Google Scholar

Y. Zhu, Y. Zhu, B.Y. Zhao, H. Zheng
Reusing 60 GHz radios for mobile radar imaging

Proceeding of the ACM 21st annual international conference on mobile computing and networking (2015), pp. 103-116
CrossRefView Record in ScopusGoogle Scholar

T.-Y.J. Kao, J. Lin

Vital sign detection using 60 GHz Doppler radar system
Proceeding of IEEE International Wireless Symp. (2013)
Google Scholar

D. Zito, D. Pepe

Mincica M, Zito F, Tognetti A, Lanatà A, De Rossi E. SoC CMOS UWB pulse Radar sensor for contactless respiratory rate monitoring
IEEE Trans. Biomed Syst Circuits, 5 (6) (2011), pp. 503-510
CrossRefView Record in ScopusGoogle Scholar

B. Neri, S. Saponara

Advances in technologies, architectures and applications of highly-integrated low-power radars
IEEE Aerosp Electron Syst Mag, 27 (1) (2012), pp. 25-36
CrossRefView Record in ScopusGoogle Scholar

E. Ragonese, A. Scuderi, V. Giammello, G. Palmisano

SiGe BiCMOS 24-GHz receiver front-end for automotive short-range radar
Analog Integr. Circuits Signal Process, 67 (2) (2011), pp. 121-130
CrossRefView Record in ScopusGoogle Scholar

V. Giammello, E. Ragonese, G. Palmisano

A 24/77-GHz SiGe BiCMOS transmitter chipset for automotive radar
Microwave Opt Technol Lett, 55 (4) (2012), pp. 782-786
Google Scholar

Texas Instruments. LMX2492/LMX2492-Q1: 14 GHz low noise fractional N PLL with ramp/chirp generation. SNAS624B. 2015.
Google Scholar

E. Gandini, M. Ettorre, R. Sauleau, A. Neto

Mutual coupling reduction of Fabry–Perot SIW feeds using a double partially reflecting pin-made grid configuration
IEEE Antennas Wireless Propag. Lett., 10 (2011), pp. 647-650
CrossRefView Record in ScopusGoogle Scholar

A. Wojtkiewicz, J. Misiurewicz, M. Nalecz, K. Jedrzejewski, K. Kulpa

Two-dimensional signal processing in FMCW radars
Proceeding of the XXth national conference on circuit and theory and electronic networks (1997), pp. 1-6
Google Scholar

W. Wang, D. Liang, Z. Wang, H. Yu, Q. Liu

Design and implementation of a FPGA and DSP Based MIMO Radar imaging system
Radioengineering, 24 (2) (2015), pp. 518-526
CrossRefView Record in ScopusGoogle Scholar

E. Hyun

Parallel and pipelined hardware implementation of radar signal processing for an FMCW multi-channel radar
Elektronika IR Electrotechnika, 21 (2) (2015), pp. 65-71
View Record in ScopusGoogle Scholar

L.E. Tirado, G. Ghazi, J.A. Martinez-Lorenzo, M.R. Carey, Y. Alvarez, F. Las Heras

A GPU implementation of the inverse fast multipole method for multi-bistatic imaging applications

Proceeding of the IEEE antennas and propagation society international symposium (2014), pp. 874-875
View Record in ScopusGoogle Scholar

C.-R. Hong, Y.-T. Hwang, W.-C. Hsu, C.-H. Chang, J.-C. Huang, H.-E. Liao

Programmable AND-CFAR signal detector design and its FPGA prototyping for FMCW radar systems
Proceeding of IEEE international symposium on VLSI design, automation and test (2011), pp. 1-4
CrossRefView Record in ScopusGoogle Scholar

SET-196 Multichannel/Multistatic Radar Imaging of Non-cooperative Targets Joint Trials, https://www.cso.nato.int/page.asp?ID=2628. 2016 [accessed 03.06.2016].
Google Scholar

B.M. Isom, J. Helvin, M. Jones, M. Knight

A new compact polarimetric solid-state X-band radar: system description and performance analysis
Proceeding of 29th conference on environmental information processing technologies (2013), pp. 1-9
View Record in ScopusGoogle Scholar

Furuno Electric. WR-2100 compact x-band dual polarimetric Doppler weather radar. http://www.furuno.com/en/systems/meteorological-monitoring/WR-2100. 2016 [accessed 03.06.2016].
Google Scholar

Sergio Saponara is Professor of Electronics at the University of Pisa, Italy, and at the Italian Naval Military Academy. He co-authored more than 250 scientific publications. He was Marie Curie Research Fellow at IMEC (B). He is associate editor of several journals from Springer, IET and MDPI and is involved in organizing committees of IEEE and SPIE conferences.

Bruno Neri is Professor of Radio-frequency Electronics at the University of Pisa, Italy. He is Director of the RF and microwave IC lab and President of the Bachelor degree and Master degree programs in Electronic Engineering at the University of Pisa. He co-authored 150 scientific publications.